

# Identification of a specific reprogramming-associated epigenetic signature in human induced pluripotent stem cells

Sergio Ruiz<sup>a,1</sup>, Dinh Diep<sup>b,c,1</sup>, Athurva Gore<sup>b</sup>, Athanasia D. Panopoulos<sup>a</sup>, Nuria Montserrat<sup>d</sup>, Nongluk Plongthongkum<sup>b</sup>, Sachin Kumar<sup>a</sup>, Ho-Lim Fung<sup>b</sup>, Alessandra Giorgetti<sup>d</sup>, Josipa Bilic<sup>d</sup>, Erika M. Batchelder<sup>a</sup>, Holm Zaehres<sup>e</sup>, Natalia G. Kan<sup>f</sup>, Hans Robert Schöler<sup>e</sup>, Mark Mercola<sup>f</sup>, Kun Zhang<sup>b,2</sup>, and Juan Carlos Izpisua Belmonte<sup>a,d,2</sup>

<sup>a</sup>Gene Expression Laboratory, Salk Institute for Biological Studies, La Jolla, CA 92037; <sup>b</sup>Department of Bioengineering, Institute for Genomic Medicine and Institute of Engineering in Medicine, and <sup>c</sup>Bioinformatics and Systems Biology Graduate Program, University of California at San Diego, La Jolla, CA 92093;

<sup>d</sup>Center of Regenerative Medicine in Barcelona, 08003 Barcelona, Spain; <sup>e</sup>Department of Cell and Developmental Biology, Max Planck Institute for Molecular Biomedicine, 48149 Münster, Germany; and <sup>f</sup>Sandford-Burnham Medical Research Institute, La Jolla, CA 92037

Edited by Kathrin Plath, University of California, Los Angeles, CA, and accepted by the Editorial Board August 23, 2012 (received for review February 10, 2012)

**Generation of human induced pluripotent stem cells (hiPSCs) by the expression of specific transcription factors depends on successful epigenetic reprogramming to a pluripotent state. Although hiPSCs and human embryonic stem cells (hESCs) display a similar epigenome, recent reports demonstrated the persistence of specific epigenetic marks from the somatic cell type of origin and aberrant methylation patterns in hiPSCs. However, it remains unknown whether the use of different somatic cell sources, encompassing variable levels of selection pressure during reprogramming, influences the level of epigenetic aberrations in hiPSCs. In this work, we characterized the epigenomic integrity of 17 hiPSC lines derived from six different cell types with varied reprogramming efficiencies. We demonstrate that epigenetic aberrations are a general feature of the hiPSC state and are independent of the somatic cell source. Interestingly, we observe that the reprogramming efficiency of somatic cell lines inversely correlates with the amount of methylation change needed to acquire pluripotency. Additionally, we determine that both shared and line-specific epigenetic aberrations in hiPSCs can directly translate into changes in gene expression in both the pluripotent and differentiated states. Significantly, our analysis of different hiPSC lines from multiple cell types of origin allow us to identify a reprogramming-specific epigenetic signature comprised of nine aberrantly methylated genes that is able to segregate hESC and hiPSC lines regardless of the somatic cell source or differentiation state.**

Induction of pluripotency in human somatic cells is an inefficient process that can be achieved by the expression of defined transcription factors (1–5). This reprogramming process involves global epigenetic remodeling and overcoming similar roadblocks present during cell transformation, which might affect genomic and epigenomic integrity (6). In fact, several recent reports have shown that human induced pluripotent stem cells (hiPSCs) contain genetic and epigenetic aberrations throughout their genome compared with their parental somatic cell populations or to human embryonic stem cells (hESCs) (7–12). For example, the analysis of whole-genome DNA methylation profiles at single-nucleotide resolution in hiPSCs, their somatic cells of origin, and hESCs revealed the presence of more than 1,000 differentially methylated regions (DMRs) between hiPSCs and hESCs (11). Moreover, this analysis, and many others, demonstrated both the persistence of specific epigenetic marks from the somatic cell of origin (residual methylation) and the acquisition of unique methylation patterns in mouse iPSCs (miPSCs) and hiPSCs (11, 13–21). Interestingly, hiPSC lines also show incomplete reprogramming of non-CG methylation in regions proximal to telomeres and centromeres (11). Altogether, these epigenetic aberrations might explain some of the observed transcriptional variation between hESC and hiPSC lines (22–24). In one of the most comprehensive reports to date, Bock et al. (23) characterized a panel of 20 hESC and 12 hiPSC lines to demonstrate that despite their global similarity, a number of genes

in each pluripotent cell line deviated from the normal expected variation compared with the DNA methylation and gene expression levels observed in the other pluripotent cell lines. Interestingly, they reported that no apparent epigenetic deviation was unique to all hiPSC lines (23). Altogether, these findings demonstrate that hiPSCs contain epigenetic aberrations. However, a majority of these reports predominantly used fibroblast-derived hiPSC lines and, thus, it remains unknown whether the use of alternative somatic cell types with variable levels of selection pressure for reprogramming might result in hiPSC lines containing fewer (or perhaps none) of these epigenetic alterations. Furthermore, although it has been shown that aberrantly methylated CpG sites are transmitted to differentiated cells (11), it remains unclear whether these epigenetic aberrancies result in transcriptional variation after differentiation.

In this work, we characterize at single nucleotide resolution the methylation profile of 17 hiPSC lines derived from six different somatic cell types with varied reprogramming efficiencies. Our results show that, independent of the somatic cell source used for reprogramming, all hiPSC lines analyzed contain abnormal epigenetic patterns. We determine that a majority of these aberrantly methylated CpG sites are transmitted to differentiated cells and can be associated with changes in gene expression after differentiation. Importantly, we identify a reprogramming-associated epigenetic signature comprised of nine aberrantly methylated genes that can segregate hESC and hiPSC lines both in the pluripotent state and after differentiation. These observations will contribute to a deeper understanding of the reprogramming process and underscore the need for a rigorous evaluation of the epigenetic integrity of hiPSC lines.

## Results

**Reprogramming Efficiency Inversely Correlates with the Percentage of Epigenetic Modifications Observed After Reprogramming.** To gain insight into the epigenetic integrity of hiPSCs, we performed targeted bisulfite sequencing with padlock probes (25, 26) to analyze the methylomes of 17 hiPSC lines, their 6 somatic cell

Author contributions: S.R., D.D., A. Gore, K.Z., and J.C.I.B. designed research; S.R., D.D., A. Gore, A.D.P., N.M., N.P., H.-L.F., A. Giorgetti, J.B., E.M.B., N.G.K., and M.M. performed research; H.Z. and H.R.S. contributed new reagents/analytic tools; S.K. analyzed data; and S.R., D.D., A. Gore, A.D.P., K.Z., and J.C.I.B. wrote the paper.

The authors declare no conflict of interest.

This article is a PNAS Direct Submission. K.P. is a guest editor invited by the Editorial Board.

The array as well as the methylation data reported in this paper have been deposited in the Gene Expression Omnibus (GEO database), [www.ncbi.nlm.nih.gov/geo](http://www.ncbi.nlm.nih.gov/geo) (accession nos. [GSE39210](https://www.ncbi.nlm.nih.gov/geo/query/acc.cgi?acc=GSE39210) and [GSE40372](https://www.ncbi.nlm.nih.gov/geo/query/acc.cgi?acc=GSE40372)).

<sup>1</sup>S.R. and D.D. contributed equally to this work.

<sup>2</sup>To whom correspondence may be addressed. E-mail: [belmonte@salk.edu](mailto:belmonte@salk.edu) or [kzhang@bioeng.ucsd.edu](mailto:kzhang@bioeng.ucsd.edu).

This article contains supporting information online at [www.pnas.org/lookup/suppl/doi:10.1073/pnas.1202352109/-DCSupplemental](http://www.pnas.org/lookup/suppl/doi:10.1073/pnas.1202352109/-DCSupplemental).

types of origin, and 7 hESC lines (*SI Text*, Fig. S1, and Table S1). We designed and synthesized a set of 330,000 synthetic probes targeting ~140,000 genomic regions known to be differentially methylated across different cell types (12, 27, 28) and additional functional regions. We determined the absolute methylation levels for an average of ~529,000 CpG sites per sample (Table S1). Although only ~1% of the human genome was covered by this assay, these preselected CpG sites were more than twice as informative as typical sites in CpG islands characterized by using lower resolution sequencing or in previously used bisulfite sequencing methods (Table S2). Unbiased hierarchical clustering of global methylation levels demonstrated a clear segregation of somatic cells and pluripotent cells (Fig. 1A). We also observed that hiPSC lines originating from the same somatic cell type tended to cluster together in subgroups (Fig. 1A and B), which, as reported (11, 13–21), supports the existence of residual methylation from somatic cells of origin in hiPSCs.

We analyzed the number of differentially methylated CpG sites (DMSs) in each hiPSC line by comparing each cell line to its direct somatic cell source of origin (Table S2). We observed that between 23% and 37% of CpG sites analyzed underwent a change in methylation state, with mesenchymal stem cells (MSCs) and fibroblasts requiring the most dramatic epigenetic change following reprogramming and neural stem cells (NSCs) requiring the least (Table S2). Interestingly, the percentage of DMSs after reprogramming correlated inversely with reprogramming efficiency, with cell sources undergoing the fewest epigenetic modifications reprogramming at higher efficiency (Fig. 1C). Moreover, we confirmed previous findings (11) and determined that, independent of somatic cell source, the global change in methylation observed after reprogramming is toward a more methylated state (Fig. S2A). Next, we investigated whether different somatic cell sources shared a core set of DMSs that might be essential to epigenetically reprogram to a pluripotent state. In fact, we observed that ~5,700 DMSs were shared among all hiPSC lines (Fig. S2B). Analysis of Gene Ontology for genes that could potentially be regulated by these DMSs revealed that genes with hypomethylated DMSs appeared to be enriched for cell signaling, protein refolding, cell metabolism, and neuronal development, whereas genes with hypermethylated DMSs appeared to be enriched for cell-cell adhesion and receptor behavior (Dataset S1).

**hiPSC Lines Share a Core Set of Aberrantly Methylated Genes That Segregate Them from hESCs.** We compared the methylation state at each CpG site in individual hiPSC lines to that of their parental source and seven hESC lines. Using an algorithm based on the  $\chi^2$  test with multiple testing corrections, we identified sites where hiPSC lines carried a methylation pattern significantly different from hESC lines (*SI Materials and Methods*). hiPSC lines derived from the same somatic cell source carried similar, although not identical, aberrant methylation patterns and clustered together based on methylation level at aberrant sites (Fig. 2A). We categorized the aberrantly methylated CpG sites into two categories: residual methylation, where the CpG site in a hiPSC line retains the methylation level of its parental cell instead of reaching the level observed in hESCs (Fig. 2B), and de novo methylation, where the CpG site in a hiPSC line acquires a methylation state found neither in its somatic source nor in hESCs (Fig. 2B). We determined that the percentage of aberrant CpG sites varied between 0.92% and 3.82% across the hiPSC lines analyzed. Furthermore, the percentage of CpG sites that showed residual methylation or de novo methylation varied between 0.32% and 1.60% and 0.57% and 2.98%, respectively (Table 1). Although we did not find a direct correlation between the amount of aberrant methylation and reprogramming efficiency or somatic cell type, we noted that some cell types appeared to possess lower aberrant methylation levels (e.g., astrocyte-derived lines) compared with others (e.g., fibroblast-derived lines) (Table 1). We determined that most aberrantly methylated CpG sites showing de novo methylation were characterized by excessive methylation after reprogramming (Fig. 2C), whereas most aber-

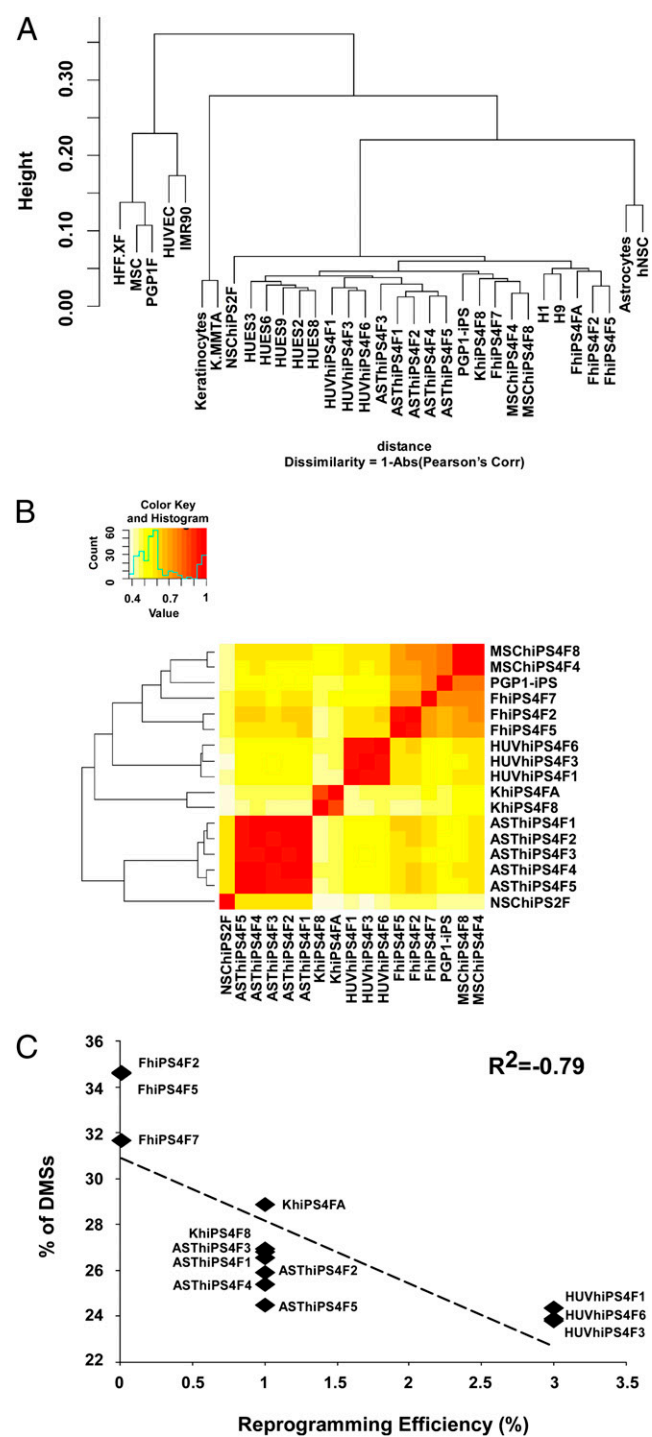


**Fig. 1.** Identification and classification of the epigenetic changes occurring during cell reprogramming. (A) Hierarchical clustering of the indicated cell lines based on the methylation state of all characterized CpG sites. HUVEC, human umbilical vein endothelial cell; K-MMTA, keratinocyte cell line; MSC, mesenchymal stem cell; NSC, neural stem cell; PGP1F, HFF,XF, IMR90, fibroblasts lines. (B) Heatmap and ordered dendrogram for all hiPSC lines based on the level of relative change observed at each differentially methylated site compared with the values observed in each respective somatic cell of origin. Pearson's correlation values were used to generate a single distance metric. (C) Reprogramming efficiency of somatic cell lines estimated after hiPSCs generation by retroviral infection of OCT4, SOX2, KLF4, and cMYC inversely correlates with the percentage of differential methylation achieved in hiPSC lines. Note that amount of epigenetic reorganization required appears to be a barrier to reprogramming.  $R^2$ , Pearson's correlation value.

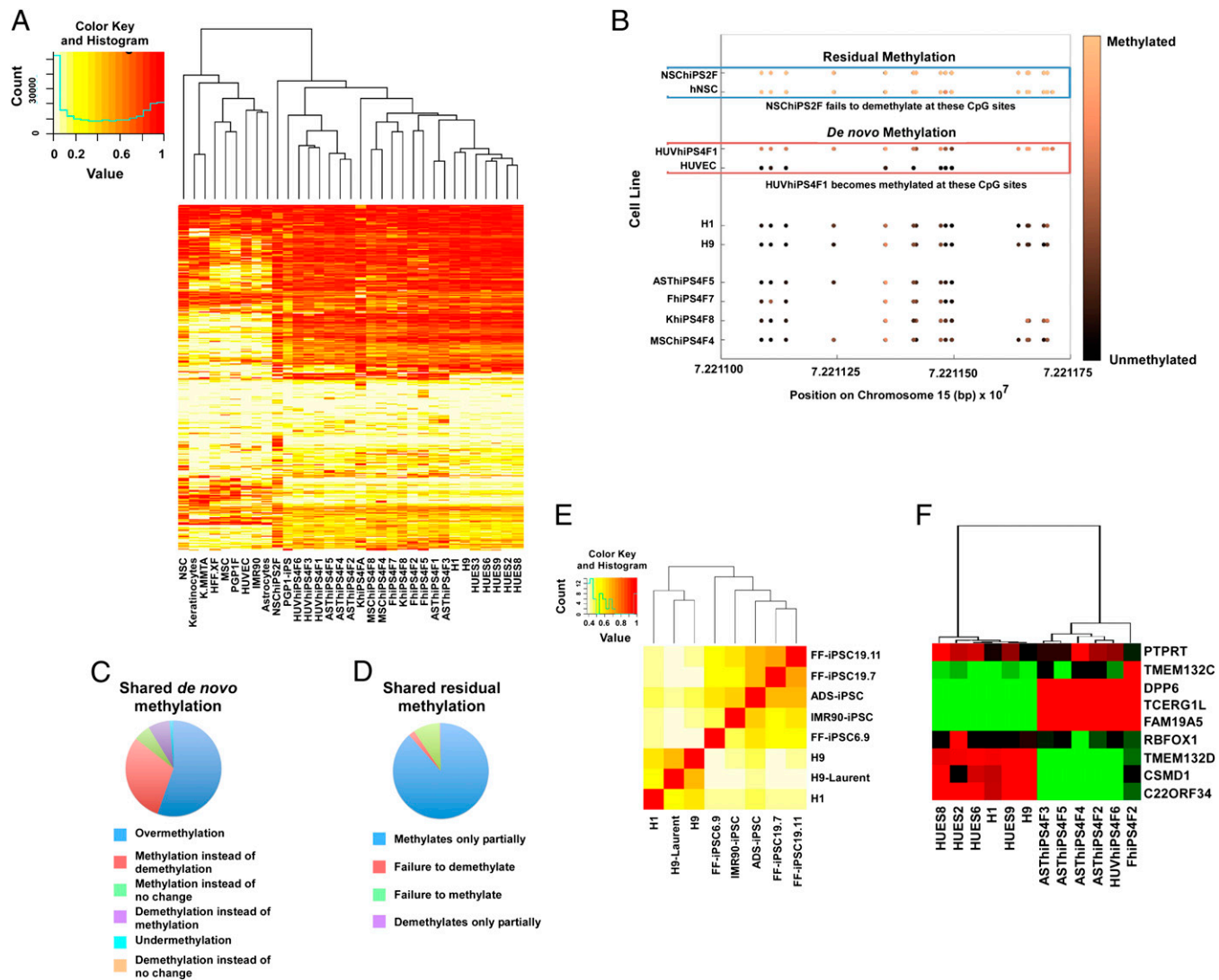


**Fig. 2.** Pluripotent cells can be segregated based on the methylation/gene expression level of nine genes. (A) Heatmap and hierarchical clustering results of the cell lines used in this study using methylation patterns at CpG sites containing aberrant methylation in at least one hiPSC line. Similar aberrant epigenetic patterns were observed in hiPSCs derived from common somatic sources, and these lines accordingly tend to cluster together. (B) Graphical representation of an example of residual methylation and de novo methylation located on chromosome 15 (*ISLR2* gene). Each circle corresponds to an individual CpG site and the level of methylation is represented in a colored pattern. In the example shown, NSChiP52F retains the epigenetic pattern of its somatic progenitor (hNSC), showing residual methylation. HUVhiP54F1 takes on an epigenetic pattern not observed in its somatic progenitor or any of the other pluripotent lines, showing a hiPSC line-specific de novo methylation. Methylation levels of the same CpG sites in hESC and hiPSC lines were included for comparison. (C and D) Types of methylation errors leading to epigenetic aberrations. Most aberrantly methylated CpG sites associated to genes showing de novo methylation (C) and residual methylation (D) in all hiPSC lines are characterized by overmethylation or partial methylation, respectively. (E) Heatmap and ordered dendrogram for the hiPSC and hESC described lines (11) based on the level of relative change observed at CpG sites associated to our nine signature genes. Note that hESC and hiPSC lines segregated in two different groups. (F) Hierarchical clustering of six hiPSC (ASThiP54F2, 3, 4, and 5, HUVhiP54F6, and FhiP4F2) and six hESC (H1, H9, HUES2, HUES6, HUES8, and HUES9) lines based on the gene expression level analyzed by real-time PCR of the nine common aberrantly methylated genes identified in hiPSC lines used in this study.

rantly methylated CpG sites associated with genes showing residual methylation were characterized by only partial methylation occurring after reprogramming (Fig. 2D).

To gain insight into potential functional consequences of these epigenetic aberrations, we linked each aberrant CpG site with its closest gene (*SI Materials and Methods*) and used this subset of genes for further analysis. Interestingly, we observed that a very small number of genes contained aberrant methylation patterns in nearly all hiPSC lines assayed in our study (16/17 hiPSC lines) regardless of somatic cell source (*Dataset S2*). We hypothesized that the nine genes (*PTPRT*, *TMEM132C*, *TMEM132D*, *TCERG1L*, *DPP6*, *FAM19A5*, *RBFOX1*, *CSMD1*, and *C22ORF34*) we identified might represent a core set of aberrantly methylated

genes that can systematically distinguish hiPSC and hESC lines. Thus, we performed unbiased hierarchical clustering based on the methylation status of CpG sites associated to this small subset of genes in previously published independent methylation datasets. Specifically, we first examined a set of whole-genome bisulfite sequencing data performed in three hESC and five hiPSC lines (11). We found that, similar to what we observed for our dataset, the methylation level of CpG sites associated to the nine genes was able to clearly segregate hESC and hiPSC lines into two distinct groups (Fig. 2E). Additionally, we used a recently published dataset that profiled the genome-wide DNA methylation level for more than 450,000 CpG sites in 19 hESC and 29 hiPSC lines (13) and observed that, despite the lower

**Table 1.** Summary of CpG sites containing residual methylation and de novo methylation in targeted regions

Cell line	Testable sites	% aberrant	% memory	% mutation	No. of genes potentially affected by memory	No. of genes potentially affected by mutation
ASThiPS4F4	434388	1.02	0.45	0.57	191	182
ASThiPS4F5	437266	0.92	0.35	0.58	211	186
ASThiPS4F1	404245	1.30	0.35	0.96	189	310
ASThiPS4F2	380656	1.16	0.41	0.75	171	243
ASThiPS4F3	343025	2.07	0.41	1.65	219	616
FhiPS4F7	340395	2.53	1.27	1.25	487	591
HUVhiPS4F1	374103	1.33	0.38	0.95	200	474
HUVhiPS4F3	392482	1.41	0.42	0.99	251	588
HUVhiPS4F6	433768	1.29	0.32	0.97	190	455
FhiPS4F2	354763	1.62	0.52	1.10	292	213
FhiPS4F5	296451	2.47	0.62	1.85	362	682
KhiPS4F8	396085	2.60	0.82	1.78	586	1040
KhiPS4FA	270126	2.41	0.46	1.95	288	831
MSChiPS4F4	437957	2.34	0.96	1.39	560	462
MSChiPS4F8	429575	2.85	1.60	1.25	896	552
NSChiPS2F	327308	3.82	0.84	2.98	538	1912
PGP1-iPS	437433	2.63	1.47	1.16	997	703

Aberrantly (residual and de novo) methylated CpG sites were classified as such when showing at least a 0.2 change in absolute methylation level and considered to have methylation levels from different underlying distributions by the  $\chi^2$  test (with Benjamini-Hochberg multiple testing correction, FDR = 0.01). Genes potentially affected by aberrantly methylated CpG sites were defined as described in *SI Materials and Methods*.

resolution, a similar clustering analysis clearly segregated all but two hiPSC lines from hESC lines (Fig. S3A).

Next, we investigated whether our core set of aberrantly methylated genes showed differential gene expression in hiPSC lines compared with hESC lines by performing real-time PCR analysis on RNA obtained from six hiPSC lines and six hESC lines (a description of the primers used in this study can be found in *Table S3*). An unbiased hierarchical clustering of the real-time PCR data results examining the gene expression of the nine shared aberrantly methylated genes demonstrated a clear segregation between hiPSC and hESC lines (Fig. 2F). Furthermore, to determine the global relevance of these findings, we also performed a similar unbiased hierarchical clustering by using previously reported independent datasets containing a variety of hESC and hiPSC lines (a total of 12 datasets). Overall, when examining the expression of these nine genes, we determined that although clear outliers and different subgroups among hiPSC lines were detected, a majority of the dataset clusters showed separation between hiPSC and hESC lines (Fig. S3B and C and *Dataset S2*). These combined results suggest the existence of shared epigenetic aberrancies associated to a small subset of genes in hiPSC lines. The validation of these aberrancies by using our data and data from independent laboratories strongly corroborates the strength of our findings.

**Aberrant Methylation at CpG Sites Is Transmitted During hiPSC Differentiation, Resulting in Transcriptional Changes Compared with Differentiated hESCs.** To further test whether the aberrant methylation and gene expression levels observed in hiPSC lines were maintained after loss of the pluripotent state, we differentiated five hESC lines and five hiPSC lines toward two different germ cell layers, endoderm and trophectoderm, by using Activin-A and BMP4, respectively. We then performed targeted bisulfite sequencing to analyze the methylomes of the hESC and hiPSC lines in their pluripotent and differentiated states (*Table S1*). In addition, the gene expression levels of H9, HUVhiPS4F1 and HUVhiPS4F3 were profiled in duplicate by using Affymetrix ST 1.0 microarrays. Between 0.3% and 1% of CpG sites were aberrantly methylated in the hiPSC lines with respect to hESC lines (*Dataset S3*). We first investigated whether these epigenetic aberrations resulted in changes in gene expression in undifferentiated cells. We observed that between 3% and 7% of genes linked to these aberrantly methylated sites showed differential gene

expression in hiPSC lines compared with hESC lines (Fig. S4A and *Dataset S3*). Additionally, we tested the expression of five genes with line-specific epigenetic de novo methylation in HUVhiPS4F1 and observed that these genes also showed differential gene expression compared with other hiPSC or hESC lines (Fig. S4B). Taken together, these results indicate that some epigenetic aberrations are associated with changes in gene expression levels.

We next analyzed the methylation status of the aberrant CpG sites in both hiPSCs and hESCs after each differentiation protocol. The CpG sites were classified based on their postdifferentiation methylation status into four categories (see Fig. 3 for a detailed description; *Dataset S3*). We observed that ~20–50% of the aberrantly methylated CpG sites detected in hiPSC lines remained aberrant after differentiation into either of the two separate cell lineages (Fig. 3A). Importantly, we observed that a subset of genes associated with these CpG sites showing differential gene expression level in undifferentiated hiPSCs compared with hESCs still remain in that condition regardless of differentiation protocol (Fig. 3B, Fig. S4C, and *Dataset S3*). Finally, to further validate the potential of the identified hiPSC-specific epigenetic signature described above, we clustered the pluripotent cells and their differentiated progenies based on both the methylation level and transcriptional abundance of the nine signature genes (Fig. 3C and D and Fig. S4D). Interestingly, the samples segregated based on whether the progenitor line was a hiPSC or hESC, and clustered by specific cell line but not by differentiation protocol. Altogether, these data suggest that the methylation and gene expression levels of the aberrantly methylated genes in hiPSC lines still segregate hESCs and hiPSCs even after differentiation toward independent germ cell layers.

## Discussion

In this work, we have used an expanded bisulfite padlock probe set to interrogate the methylation level of targeted CpG sites identified to carry differential methylation in various cell states regardless of CpG density (12, 26–28). This unique approach identified genes linked to individual aberrantly methylated CpG sites that are not necessarily located in CpG-enriched genomic regions. Our results show that epigenetic aberrations occur in hiPSCs regardless of the somatic cell type of origin. We demonstrated that aberrant epigenetic patterns in hiPSC lines influence gene expression and could explain functional diversity

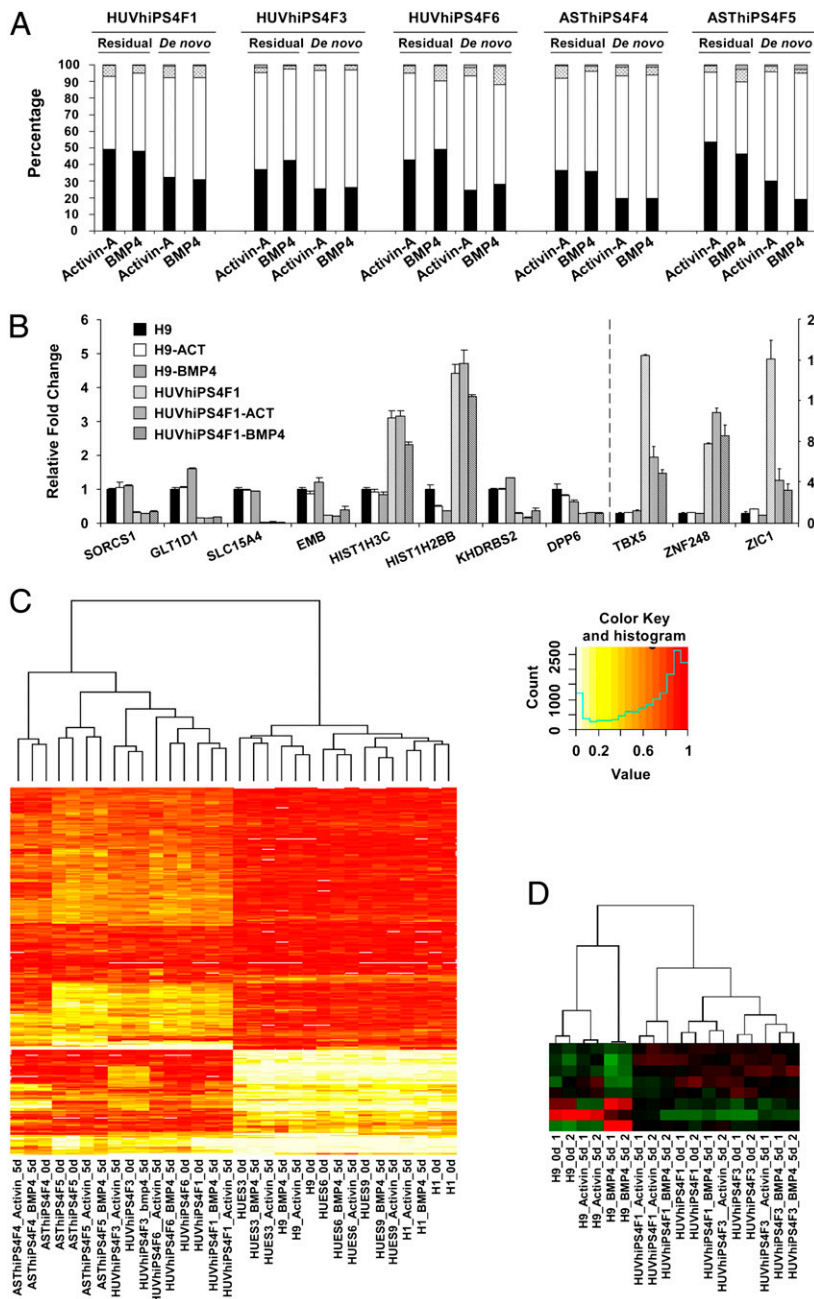


**Fig. 3.** Reprogramming-associated epigenetic/transcriptional signatures segregate hiPSCs and hESCs after differentiation. (A) Percentage of aberrant CpG sites identified between hESC-derived lines and the corresponding hiPSC-derived lines classified in the following categories: aberrant methylation remains and is still aberrant compared with differentiated hESCs (A); aberrant methylation remains but is the same as the one found in differentiated hESCs (B); aberrant methylation is removed during differentiation reaching the level found in differentiated hESCs (C); and aberrant methylation changed to a new aberrant methylation state (D). (B) Genes with aberrantly methylated CpG sites and differential transcriptional abundance with at least a twofold cutoff were identified in the HUVhiPS4F1 cell line after comparison with H9 cells. Graph shows the relative fold change in the expression of genes still aberrantly methylated after differentiation between the differentiated HUVhiPS4F1 cell line and the differentiated hESC cell line. Note that differential expression was independent on whether Activin or BMP4-differentiated cells were analyzed. (C) Hierarchical clustering of hESC (H1, H9, HUES3, HUES6, and HUES9) and hiPSC (HUVhiPS4F1, HUVhiPS4F3, HUVhiPS4F6, ASThiPS4F4, and ASThiPS4F5) lines in their pluripotent and differentiated states based on the methylation level of the nine common aberrantly methylated genes identified in the hiPSC lines used in this study. (D) Hierarchical clustering of hESC (H9) and hiPSC (HUVhiPS4F1 and HUVhiPS4F3) lines in their pluripotent and differentiated states based on the gene expression level of the nine common aberrantly methylated genes identified in the hiPSC lines used in this study. Data were obtained from microarray analysis.

within hiPSC lines and between hiPSC and hESC lines (29–31). In fact, we observed the existence of genes aberrantly methylated and differentially expressed in hiPSC lines compared with hESCs that still remained in that condition after differentiation regardless of differentiation protocol.

The use of hiPSC lines derived from six different somatic cell types enabled us to narrow down a precise core set of genes that contained aberrant epigenetic patterns associated with the hiPSC state. This analysis led us to identify a reprogramming-associated epigenetic signature based on the methylation level of nine genes that could segregate hESC and hiPSC lines in both the pluripotent state and after differentiation. There have been many reports suggesting the existence of epigenetic and transcriptional differences between hiPSC and hESC lines (11–24). Interestingly, recently reported analysis using restricted representation bisulfite sequencing (RRBS) showed that although cell line-specific outliers at both the methylation and gene expression levels could be

identified, no apparent epigenetic deviation was unique to all hiPSC lines (23). However, the data presented therein (23) did not appear to target any of the aberrantly methylated CpG sites covered in our hiPSC-specific signature, because RRBS mainly focuses on the analysis of CpG islands (resulting in low coverage of genomic regions with low CpG density, including many functional elements such as enhancers). When we compared the lists of CpG sites associated with the nine genes characterized by our dataset to the Bock et al. dataset (23), there was almost no overlap between the two sets of analyzed CpG sites. In fact, in the Bock et al. dataset (23), only 1 CpG site of the ~600 we identified as aberrantly methylated CpG sites associated to the 9 genes was included in their analysis. Thus, when we clustered the pluripotent cell lines used in the Lister et al. dataset (which analyzed a near-complete selection of CpG sites genome-wide in an unbiased manner; ref. 11) based on the CpG sites that were analyzed by the Bock et al. dataset, no clear separation was observed

between hESC and hiPSC lines. However, when we clustered the hESC and hiPSC lines included in the Lister et al. dataset based on the CpG sites analyzed in our study, we found that we were able to segregate the two different pluripotent cell types. Furthermore, when we compared our data to an extensive set of genome-wide DNA methylation profiling of hESC and hiPSC lines, that had analyzed CpG sites that overlapped with our dataset (13), we were again able to separate these pluripotent cell lines based on our identified hiPSC-specific epigenetic signature. Altogether, these findings indicate that when characterizing the epigenetic differences between hiPSCs and hESCs, cautions must be taken to interpret the results when only a subset of genomic regions is investigated.

Furthermore, we also validated our reprogramming-associated epigenetic signature by using gene expression data from several previously reported datasets (refs. 13 and 32 and [Dataset S2](#)). We observed that a majority of independent clusters separated hiPSC and hESC lines, although clear outliers and different subgroups among hiPSC lines were detected. This result is not totally unexpected because it has been shown that gene expression levels in pluripotent cells are highly variable and depend on how pluripotent cells are generated or maintained (33). Moreover, Bock et al. (23) also reported the existence of genes in pluripotent cells that contained similar methylation levels but were associated to variable levels of gene expression. Therefore, we cannot exclude the possibility that some hiPSC lines might not segregate well from hESC lines when using the gene expression levels of these nine genes to cluster them.

Finally, although the genes *TMEM132D*, *FAM19A5*, and *TCERG1L* have been reported to be involved in neural processes, we did not identify any significant functional enrichment associated with the nine genes aberrantly methylated in hiPSC lines. Interestingly, Lister et al. (11) identified five of our nine genes (*TMEM132C*, *TMEM132D*, *FAM19A5*, *DPP6*, and *TCERG1L*) located within non-CG mega-DMRs as clear outliers in terms of gene expression compared with hESCs. In fact, up to half of their gene outliers located within non-CG mega-DMRs (11) were

observed aberrantly methylated in 14 of the 17 hiPSC used in this study ([Dataset S3](#)). Further studies will be needed to better clarify the role of non-CG mega-DMRs and their implication in the functional behavior of hiPSCs compared with hESCs.

Overall, the results shown here demonstrate the existence of intrinsic common reprogramming-associated epigenetic differences associated with the hiPSC state. We demonstrated that the epigenetic signature described in this work, based on the methylation level of nine genes, can segregate hiPSC and hESC lines in both the pluripotent state and after differentiation and could explain some of the functional differences between these two pluripotent cell types.

## Materials and Methods

**Cell Culture.** Human H9 (WA09), H1 (WA01), HUES2, HUES3, HUES6, HUES8, and HUES9 embryonic stem cell lines were obtained from WiCell Research Institute or Harvard University and maintained as described (34). Derived hiPSCs were cultured as described (34). IMR90 human fibroblasts (ATCC; CCL-186) and 293T cells were cultured in DMEM (Invitrogen) supplemented with 10% FBS and 0.1 mM nonessential amino acids. HUVEC cells were obtained from Lonza (C-2519A) and grown with EGM-2 media (Lonza) as recommended. MSCs were kindly provided by Cécile Volle (Sanofi-Aventis, Toulouse, France) and grown in α-MEM (Invitrogen) containing 10% FBS (HyClone), penicillin/streptomycin, sodium pyruvate, nonessential amino acids, and L-glutamine (all from Invitrogen). Human keratinocytes were obtained and cultured as described (35).

Additional experimental and data analysis procedures are provided in [SI Materials and Methods](#).

**ACKNOWLEDGMENTS.** We thank the J.C.I.B. and K.Z. laboratories for helpful discussions and to Dr. Travis Berggren, Margaret Lutz, and Veronica Modesto for their support at the Salk Institute-Stem Cell Core. S.R. was partially supported by Instituto de Salud Carlos III Grant CGCV-1335/07-3. A.G. was supported by the Focht-Powell Fellowship and a California Institute for Regenerative Medicine (CIRM) Predoctoral Fellowship. A.D.P. was partially supported by National Institutes of Health (NIH) Training Grant T32 CA009370. Work in this manuscript was supported by grants from Fundacion Cellex, Ministerio de Economía y Competitividad (MINECO), Sanofi, the G. Harold and Leila Y. Mathers Charitable Foundation, and The Leona M. and Harry B. Helmsley Charitable Trust, California Institute for Regenerative Medicine Grants RB3-05083 and TR1-01273, and NIH Grant R01 GM097253.

1. Takahashi K, et al. (2007) Induction of pluripotent stem cells from adult human fibroblasts by defined factors. *Cell* 131:861–872.
2. Yu J, et al. (2007) Induced pluripotent stem cell lines derived from human somatic cells. *Science* 318:1917–1920.
3. Lowry WE, et al. (2008) Generation of human induced pluripotent stem cells from dermal fibroblasts. *Proc Natl Acad Sci USA* 105:2883–2888.
4. Meissner A, Wernig M, Jaenisch R (2007) Direct reprogramming of genetically unmodified fibroblasts into pluripotent stem cells. *Nat Biotechnol* 25:1177–1181.
5. Park IH, et al. (2008) Reprogramming of human somatic cells to pluripotency with defined factors. *Nature* 451:141–146.
6. Daley GQ (2008) Common themes of dedifferentiation in somatic cell reprogramming and cancer. *Cold Spring Harb Symp Quant Biol* 73:171–174.
7. Hussein SMI, et al. (2011) Copy number variation and selection during reprogramming to pluripotency. *Nature* 471:58–62.
8. Laurent LC, et al. (2011) Dynamic changes in the copy number of pluripotency and cell proliferation genes in human ESCs and iPSCs during reprogramming and time in culture. *Cell Stem Cell* 8:106–118.
9. Gore A, et al. (2011) Somatic coding mutations in human induced pluripotent stem cells. *Nature* 471:63–67.
10. Mayshar Y, et al. (2010) Identification and classification of chromosomal aberrations in human induced pluripotent stem cells. *Cell Stem Cell* 7:521–531.
11. Lister R, et al. (2011) Hotspots of aberrant epigenetic reprogramming in human induced pluripotent stem cells. *Nature* 471:86–73.
12. Doi A, et al. (2009) Differential methylation of tissue- and cancer-specific CpG island shores distinguishes human induced pluripotent stem cells, embryonic stem cells and fibroblasts. *Nat Genet* 41:1350–1353.
13. Nazer KL, et al. (2012) Recurrent variations in DNA methylation in human pluripotent stem cells and their differentiated derivatives. *Cell Stem Cell* 10:620–634.
14. Marchetto MC, et al. (2009) Transcriptional signature and memory retention of human-induced pluripotent stem cells. *PLoS ONE* 4:e7076.
15. Ohi Y, et al. (2011) Incomplete DNA methylation underlies a transcriptional memory of somatic cells in human iPSCs. *Nat Cell Biol* 13:541–549.
16. Bar-Nur O, Russ HA, Efrat S, Benvenisty N (2011) Epigenetic memory and preferential lineage-specific differentiation in induced pluripotent stem cells derived from human pancreatic islet beta cells. *Cell Stem Cell* 9:17–23.
17. Polo JM, et al. (2010) Cell type of origin influences the molecular and functional properties of mouse induced pluripotent stem cells. *Nat Biotechnol* 28:848–855.
18. Kim K, et al. (2010) Epigenetic memory in induced pluripotent stem cells. *Nature* 467:285–290.
19. Kim K, et al. (2011) Donor cell type can influence the epigenome and differentiation potential of human induced pluripotent stem cells. *Nat Biotechnol* 29:1117–1119.
20. Quattrociemi M, et al. (2011) Intrinsic cell memory reinforces myogenic commitment of pericyte-derived iPSCs. *J Pathol* 223:593–603.
21. Hu Q, Friedrich AM, Johnson LV, Clegg DO (2010) Memory in induced pluripotent stem cells: Reprogrammed human retinal-pigmented epithelial cells show tendency for spontaneous redifferentiation. *Stem Cells* 28:1981–1991.
22. Chin MH, et al. (2009) Induced pluripotent stem cells and embryonic stem cells are distinguished by gene expression signatures. *Cell Stem Cell* 5:111–123.
23. Bock C, et al. (2011) Reference Maps of human ES and iPS cell variation enable high-throughput characterization of pluripotent cell lines. *Cell* 144:439–452.
24. Ghosh Z, et al. (2010) Persistent donor cell gene expression among human induced pluripotent stem cells contributes to differences with human embryonic stem cells. *PLoS ONE* 5:e8975.
25. Deng J, et al. (2009) Targeted bisulfite sequencing reveals changes in DNA methylation associated with nuclear reprogramming. *Nat Biotechnol* 27:353–360.
26. Diep D, et al. (2012) Library-free methylation sequencing with bisulfite padlock probes. *Nat Methods* 9:270–272.
27. Irizarry RA, et al. (2009) The human colon cancer methylome shows similar hypo- and hypermethylation at conserved tissue-specific CpG island shores. *Nat Genet* 41:178–186.
28. Lister R, et al. (2009) Human DNA methylomes at base resolution show widespread epigenomic differences. *Nature* 462:315–322.
29. Miura K, et al. (2009) Variation in the safety of induced pluripotent stem cell lines. *Nat Biotechnol* 27:743–745.
30. Feng Q, et al. (2010) Hemangioblastic derivatives from human induced pluripotent stem cells exhibit limited expansion and early senescence. *Stem Cells* 28:704–712.
31. Hu BY, et al. (2010) Neural differentiation of human induced pluripotent stem cells follows developmental principles but with variable potency. *Proc Natl Acad Sci USA* 107:4335–4340.
32. Yu J, et al. (2009) Human induced pluripotent stem cells free of vector and transgene sequences. *Science* 324:797–801.
33. Newman AM, Cooper JB (2010) Lab-specific gene expression signatures in pluripotent stem cells. *Cell Stem Cell* 7:258–262.
34. Ruiz S, et al. (2011) A high proliferation rate is required for cell reprogramming and maintenance of human embryonic stem cell identity. *Curr Biol* 21:45–52.
35. Aasen T, et al. (2008) Efficient and rapid generation of induced pluripotent stem cells from human keratinocytes. *Nat Biotechnol* 26:1276–1284.

# Supporting Information

Ruiz et al. 10.1073/pnas.1202352109

## SI Text

Three of the somatic cell types [human umbilical vein endothelial cells (HUVECs), astrocytes, and neural stem cells (NSCs)] were of fetal/neonatal origin, keratinocytes were obtained from a 5-y-old individual, mesenchymal stem cells (MSCs) were obtained from liposuctioned tissue from aged women and Fibroblasts (HFF.XF and PGP1F) were obtained from two different biopsies from a 55-y-old and a 5-y-old individual (Table S1). Young cell sources were preferentially chosen to rule out age-accrued DNA damage or epigenetic alterations as a possible source of aberrations, because these cell samples likely possess a lower level of exposure to natural stress and mutagenic agents. Moreover, embryonic and adult stem cells (NSCs and MSCs) were specifically chosen because they have more effective mechanisms of genomic preservation than somatic cells. All hiPSC lines were generated by using retroviral or lentiviral infection to express between two and four of the reprogramming factors (see Table S1 for details). All lines were fully characterized in terms of pluripotent gene expression, transgene silencing, karyotype, and in vitro and in vivo differentiation into tissues from all three embryonic germ layers (Fig. S1) (1–5).

## SI Materials and Methods

**hiPSC Generation.** The hiPSC lines ASThiPS4F1, ASThiPS4F2, ASThiPS4F3, ASThiPS4F4, ASThiPS4F5, HUVhiPS4F1, HUVhiPS4F3, HUVhiPS4F6, FhiPS4F2, FhiPS4F5, FhiPS4F7, KhiPS4FA, PGP1-iPS, and NSChiPS2F were described (1–5), and obtained from existing cultures. To generate hiPSCs (KhiPS4F8, MSChiPS4F4, and MSChiPS4), experiments were performed as described with minor modifications (6). Briefly, keratinocytes or MSCs were infected with an equal ratio of retroviruses by spinfection of the cells at  $800 \times g$  for 1 h at room temperature in the presence of polybrene (4  $\mu$ g/mL). After two (for keratinocytes) or three (for MSCs) viral infections, cells were trypsinized and transferred onto fresh irradiated mouse embryonic or human fibroblasts (iMEFs or iHFs), respectively. One day after, cells were switched to hESC medium [DMEM/F12 or KO-DMEM (Invitrogen) supplemented with 20% Knockout Serum Replacement (Invitrogen), 1 mM L-glutamine, 0.1 mM nonessential amino acids, 55  $\mu$ M  $\beta$ -mercaptoethanol and 10 ng/mL bFGF (Joint Protein Central)]. For the derivation of hiPSC lines, colonies were manually picked and maintained on fresh mouse embryonic fibroblasts (MEFs) feeder layers for five passages before growth in Matrigel/mTesR1 conditions.

**Immunostaining.** Immunofluorescence analysis for the detection of pluripotent markers in hiPSCs or for the detection of differentiation-associated markers in teratomas were performed as described (4).

**RNA Isolation and Real-Time PCR Analysis.** Total RNA was isolated by using TRIzol Reagent (Invitrogen) according to the manufacturer's recommendations. cDNA was synthesized by using the SuperScript II Reverse Transcriptase kit for RT-PCR (Invitrogen) or the RT Supermix M-MuLV kit (BioPioneer). Real-time PCR was performed by using the SYBR-Green PCR Master mix (Applied Biosystems) in the ViiA 7 Real-Time PCR System (Applied Biosystems). GAPDH expression was used to normalize values of gene expression, and data are shown as fold change relative to the value of the sample control. All of the samples were done in triplicate. Primers used for real-time PCR experiments are listed in Table S3.

**Teratoma Formation and Karyotype Analysis.** Severe combined immunodeficient mice (NOD.Cg-*Prkdc*<sup>scid</sup> *Il2rg*<sup>tm1Wjl</sup>/SzJ; Jackson Laboratories) were used to test the teratoma induction capacity of the hiPSC lines as described (4). hiPSC lines grown on Matrigel were processed to perform karyotype analysis as described (4). All animal experiments were conducted by following experimental protocols approved by the Institutional Ethics Committee on Experimental Animals at the Parc de Recerca Biomedica de Barcelona (PRBB), in full compliance with Spanish and European laws and regulations.

**Bisulfite Padlock Probes Production.** Oligonucleotides were synthesized by ink-jet printing on programmable microarrays (Agilent Technologies) and released to form a combined library of 330,000 oligonucleotides. The library was prepared for padlock capture by using a described protocol (7, 8).

**Sample Preparation and Capture.** Genomic DNA was extracted by using the ALLPrep DNA/RNA Mini kit (Qiagen) and QIAamp DNA Micro kit (Qiagen). The bisulfite conversion and capture reactions were carried out on 1–1.2  $\mu$ g of each sample by using established protocols (7, 8). Briefly, DNA was bisulfite converted by using the EZ-96Methylation Gold Kit (Zymo Research). Approximately 200–300 ng of converted gDNA from each sample was captured by using prepared padlock probe oligonucleotides, resulting in a circular DNA library of targeted CpG sites.

**Bisulfite Sequencing Library Construction.** The circular DNA library was amplified as described (7) with slight modifications. Briefly, two-thirds of each capture reaction was used to prepare two real-time PCR reactions with 20 pmoles each of AmpF6.4Sol and AmpR6.3 indexing primers (Table S3) and 50  $\mu$ L of 2 $\times$  KAPA SYBR FAST Universal qPCR Master Mix (KAPA Biosystems). Thermocycling was carried out at 98 °C for 30 s; 8 cycles of 98 °C for 10 s, 58 °C for 30 s, and 72 °C for 30 s; and 12–14 cycles of 98 °C for 10 s and 72 °C for 30 s. Finally, the reactions were held at 72 °C for 3 min. Duplicate reactions were then pooled, purified by using 0.8 $\times$  AMPure magnetic beads (Agencourt), and quantified by using 6% polyacrylamide gel electrophoresis. Samples were mixed in equimolar ratios to create two libraries, and together were size selected with 6% polyacrylamide gel electrophoresis. The first pool with 60 libraries was sequenced in five lanes of a paired-end 100-bp Illumina Hi-Seq run, and the second pool with 12 libraries was sequenced in 1 lane of a paired-end 110-bp Illumina Hi-Seq run.

**Bisulfite Read Mapping and Data Analysis.** Bisulfite converted data were processed as described (7, 9). Heatmaps and dendograms were created from the Pearson's correlation matrices of (i) the relative change in methylation level between each hiPSC line and its somatic progenitor, and (ii) the absolute methylation level at each site in each line.

**Statistical Analysis/Identification of Differentially Methylated Sites.** To identify sites showing a change in methylation after reprogramming, a  $\chi^2$  test with Yates' correction was carried out on each CpG site characterized in each hiPSC line and corresponding paired somatic cell line. The Benjamini–Hochberg method was used to correct for multiple testing errors; the false discovery rate (FDR) was set at 1%. This resulted in a set of differentially methylated sites (DMSs) for each hiPSC line; at each site, the methylation level was statistically significantly different from the somatic progenitor line and different by at least a 0.2 change in

absolute methylation level. A set of 5,701 DMSs were shared by all 17 hiPSC lines and were split into two groups (hypermethylated or hypomethylated) based on the mean change in relative methylation level between somatic progenitor and hiPSC line. A total of 5,056 sites were hypermethylated and 645 sites were hypomethylated in all hiPSC lines after reprogramming. Each list of sites was tested for functional similarity by using GREAT (<http://great.stanford.edu>), along with a list of the 336,904 sites characterized in all lines as background. The single closest gene within 10 kbp of a DMS from each list, and the enriched GO Biological Process terms chart were generated by using GREAT.

**Statistical Analysis/Identification and Classification of Epigenetic Aberrations.** The following procedure was followed for all hiPSC lines to first identify aberrant CpG sites and then categorize them as residual methylation or de novo methylation. First, the methylation levels at each CpG site in the hiPSC line were considered and compared with the average methylation level and the upper and lower bounds of methylation level for the same site in the hESC lines. Those sites showing at least a 0.2 change in absolute methylation level, considered to have methylation levels from different underlying distributions by the  $\chi^2$  test (with Benjamini–Hochberg multiple testing correction; FDR = 0.01), and having a methylation level at least 0.2 away from either the maximum or the minimum hESC methylation level were considered to be “aberrantly methylated.” These aberrant CpG sites were then classified into two categories: de novo methylation and residual methylation. Sites were classified as de novo methylation if the methylation level met three conditions: the level in the hiPSC line was statistically significantly different by the same  $\chi^2$  criteria than the level in its corresponding somatic cell progenitor, the hiPSC line’s absolute methylation level was at least 0.2 away from the somatic cell line’s, and the hiPSC methylation level was not between that of its somatic progenitor and the hESC lines. Other aberrant sites were classified as residual methylation. CpG sites were associated with a gene if the gene’s transcription start or end site was located within 10 kilobases; CpG sites located more than 10 kb away from a gene were considered to be “unlinked.” In cases where multiple genes were within 10 kb, the CpG site was associated with the closest gene.

**Classification of Unique and Shared Epigenetic Aberrations.** To obtain an enriched list of genes and their associated CpG sites for functional analysis, genes that showed either “shared” or “line-specific” residual methylation and de novo methylation patterns were identified. In order for a gene to have been considered to carry “shared” residual methylation or de novo methylation patterns, it must have contained CpG sites showing residual methylation or de novo methylation in at least 16 of the 17 analyzed hiPSC lines. In order for a gene to have been considered to carry “line-specific” residual methylation or de novo methylation pat-

terns for a given hiPSC line, it must have contained CpG sites showing residual methylation or de novo methylation in no more than three other lines derived from separate progenitor cell types. This grouping resulted in lists of genes that showed aberrant methylation in either all hiPSC lines or only a few hiPSC lines and allowed us to focus on genes that could have methylation-based functional changes in expression.

**Activin-Induced Differentiation.** Cells were treated with media (mTeSR1) plus Activin-A (100 ng/mL). Media was replaced daily for 5 d. Cells were then collected with TrypLE (Invitrogen), washed with PBS, and processed for DNA and RNA isolation.

**BMP4-Induced Differentiation.** Cells were treated with BMP4 for 5 d with minor modifications as described (10). Cells were then collected with TrypLE (Invitrogen), washed with PBS, and processed for DNA and RNA isolation.

**Analysis of Epigenetic Aberrations after Differentiation.** Targeted bisulfite sequencing was performed on genomic DNA from pluripotent and differentiated cultures of hiPSC and hESC lines as described above. Aberrant methylation was called in the pluripotent hiPSC state as described above. Two comparisons were then performed for each aberrantly methylated site by using the above method to call differential methylation: the first between the hiPSC-pluripotent state and the hiPSC-differentiated state, and the second between the hESC-differentiated state, and the hiPSC-differentiated state. Based on the results of these two statistical tests, each site was characterized into one of four categories: (i) hiPSC-pluripotent and hiPSC-differentiated states are similar, but different from hESC-differentiated state; (ii) hiPSC-pluripotent state, hiPSC-differentiated, and hESC-differentiated states are all similar; (iii) hiPSC-differentiated and hESC-differentiated states are similar, and different from hiPSC-pluripotent state; or (iv) all three states are different.

**Microarray Data.** The GeneChip microarray (Affymetrix ST 1.0 microarrays) processing was performed by the Department of Functional Genomics at Salk Institute according to the manufacturer’s protocols (Affymetrix). The amplification and labeling were processed as indicated in Nugen protocol with 100 ng of starting RNA. For each sample, 3.75 mg of ssDNA were labeled and hybridized to the Affymetrix ST 1.0 chips. Expression signals were scanned on an Affymetrix GeneChip Scanner. The data extraction was done by the Affymetrix GCOS software. The analysis of the data were performed by using affylmGUI package in R-Bioconductor. Briefly, .CEL files were imported in R-bioconductor for preprocessing and normalization. Cluster 3.0 software were used to perform hierarchical clustering on RMA-normalized probeset intensity values. The array as well as the methylation data reported in this paper have been deposited in the Gene Expression Omnibus (GEO database), [www.ncbi.nlm.nih.gov/geo](http://www.ncbi.nlm.nih.gov/geo) (accession nos. GSE39210 and GSE40372).

1. Gore A, et al. (2011) Somatic coding mutations in human induced pluripotent stem cells. *Nature* 471:63–67.
2. Kim JB, et al. (2009) Direct reprogramming of human neural stem cells by OCT4. *Nature* 461:649–3.
3. Panopoulos AD, et al. (2011) Rapid and highly efficient generation of induced pluripotent stem cells from human umbilical vein endothelial cells. *PLoS ONE* 6:e19743.
4. Ruiz S, et al. (2010) High-efficient generation of induced pluripotent stem cells from human astrocytes. *PLoS ONE* 5:e15526.
5. Panopoulos AD, et al. (2012) The metabolome of induced pluripotent stem cells reveals metabolic changes occurring in somatic cell reprogramming. *Cell Res* 22:168–177.
6. Ruiz S, et al. (2011) A high proliferation rate is required for cell reprogramming and maintenance of human embryonic stem cell identity. *Curr Biol* 21:45–52.
7. Deng J, et al. (2009) Targeted bisulfite sequencing reveals changes in DNA methylation associated with nuclear reprogramming. *Nat Biotechnol* 27:353–360.
8. Diep D, et al. (2012) Library-free methylation sequencing with bisulfite padlock probes. *Nat Meth* 9:270–272.
9. Shoemaker R, Deng J, Wang W, Zhang K (2010) Allele-specific methylation is prevalent and is contributed by CpG-SNPs in the human genome. *Genome Res* 20:883–889.
10. Xu RH, et al. (2002) BMP4 initiates human embryonic stem cell differentiation to trophoblast. *Nat Biotechnol* 20:1261–1264.

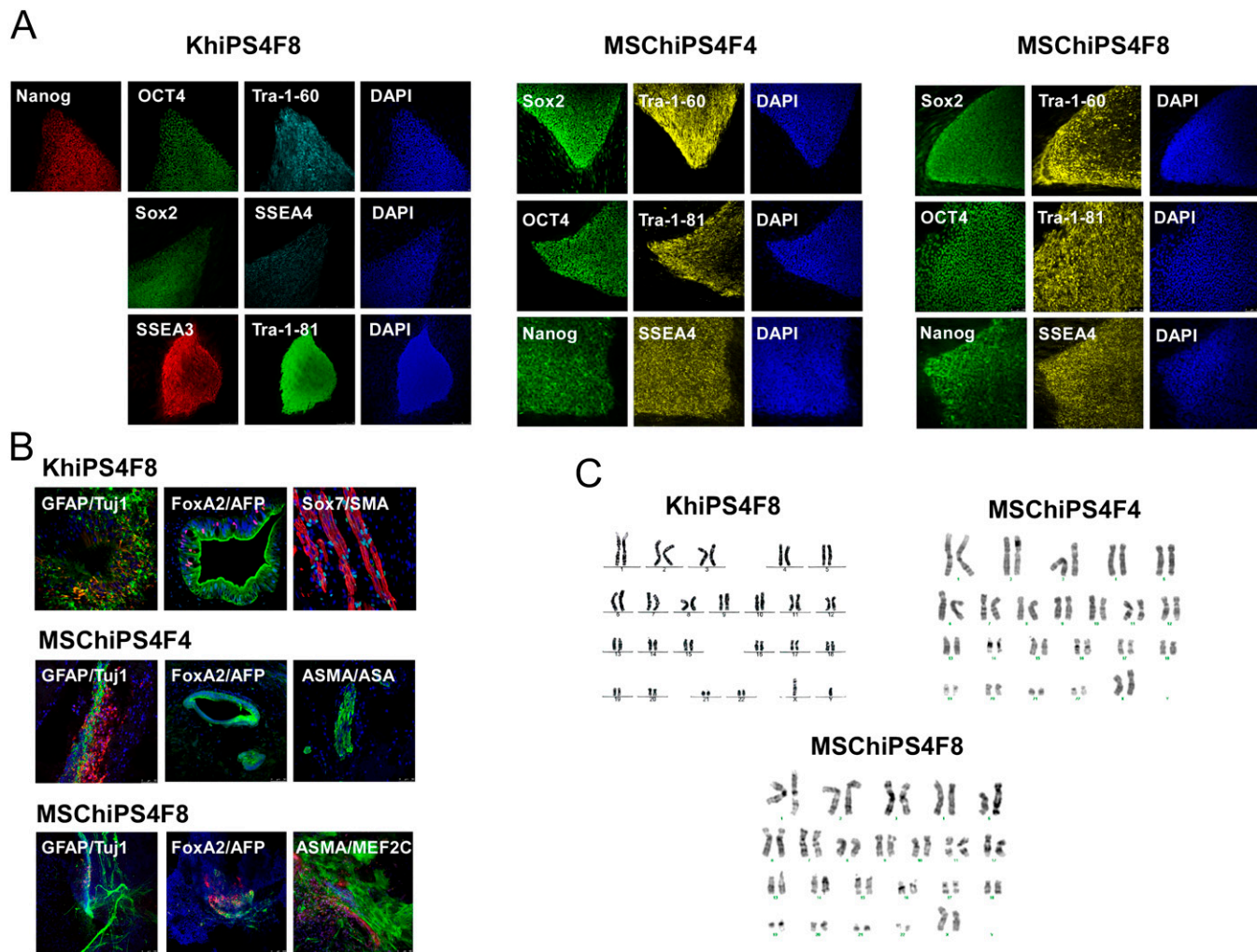


**Fig. S1.** Characterization of the hiPSC lines KhiPS4F8, MSChiPS4F4, and MSChiPS4F8. (A) Immunofluorescence analysis of the indicated pluripotent markers in the KhiPS4F8, MSChiPS4F4, and MSChiPS4F8 cell lines. (B) Differentiation potential of the KhiPS4F8, MSChiPS4F4, and MSChiPS4F8 cell lines assessed in vivo by teratoma formation after injection into the testes of SCID beige mice. Isolated teratomas contain structures that represent the three main embryonic germ layers as defined by the expression of specific endodermal ( $\alpha$ -fetoprotein, green), and FoxA2, red), ectodermal (Tuj1, green and GFAP, red), and mesodermal [SMA, red (smooth muscle actin), ASMA, red or Sox17, green] markers. All images were obtained from the same tumor. (C) Karyotype analysis of the hiPSC lines KhiPS4F8, MSChiPS4F4, and MSChiPS4F8. A normal karyotype is present in all three lines.

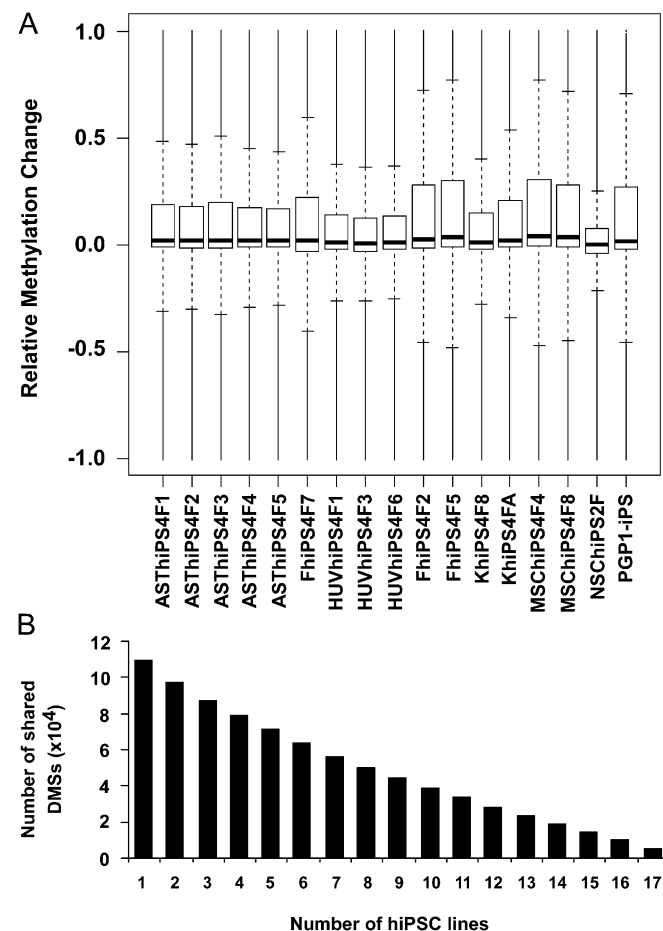


**Fig. S2.** Trends observed in differentially methylated sites (DMSs) after reprogramming. (A) Boxplots showing the methylation change observed at all CpG sites in hiPSC lines relative to their somatic progenitors after reprogramming. A  $-1$  value means that a completely methylated site becomes completely unmethylated, whereas a  $+1$  value means that a completely unmethylated site becomes completely methylated. Most CpG sites either do not change in methylation state or become more methylated after reprogramming regardless of somatic progenitor. (B) Cumulative bar plot showing the number of DMSs shared in a defined number of hiPSC lines. For instance, the number of DMSs shared in one hiPSC line represents the number of CpG sites differentially methylated in at least one hiPSC line and the number of DMSs shared in two hiPSC lines represents the number of CpG sites differentially methylated in at least two hiPSC lines. Thus, the number of DMSs shared in all hiPSC lines represents the core number of CpG sites differentially methylated during cell reprogramming regardless of somatic cell source. In these shared DMSs among all of the hiPSC lines, a total of 5,056 CpG sites were hypermethylated, whereas 645 CpG sites were hypomethylated.

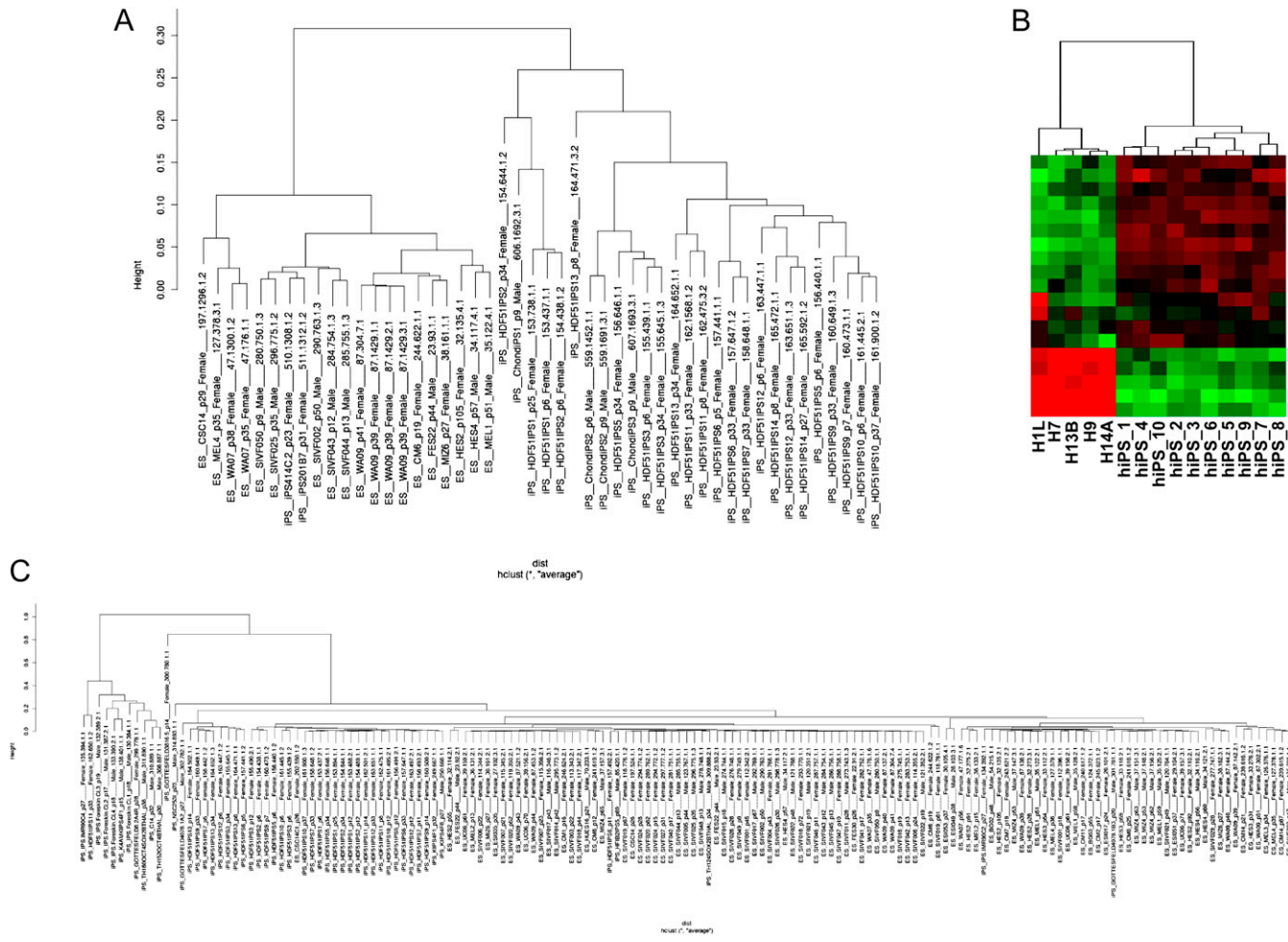


**Fig. S3.** Clustering of pluripotent cell lines based on the methylation and gene expression level of the nine aberrantly methylated genes specific to hiPSCs. (A) Ordered dendrogram for the hiPSC and hESC lines described (1) based on the level of relative change observed at methylation array probes associated with the nine signature genes identified in this study. Note that all but two hiPSC lines clearly cluster separately from hESC lines. (B) Hierarchical clustering of 10 hiPSC (hiP51-10) and 5 hESC (H1L, H9, H7, H13B, and H14A) lines (2) based on the gene expression level of the 9 common aberrantly methylated genes identified in hiPSC lines used in this study. (C) Ordered dendrogram for the hiPSC and hESC lines described (1) based on the level of relative change in gene expression level of the nine signature genes identified in this study.

1. Nazor KL, et al. (2012) Recurrent variations in DNA methylation in human pluripotent stem cells and their differentiated derivatives. *Cell Stem Cell* 10:620-634.
2. Yu J, et al. (2009) Human induced pluripotent stem cells free of vector and transgene sequences. *Science* 324:797-801.

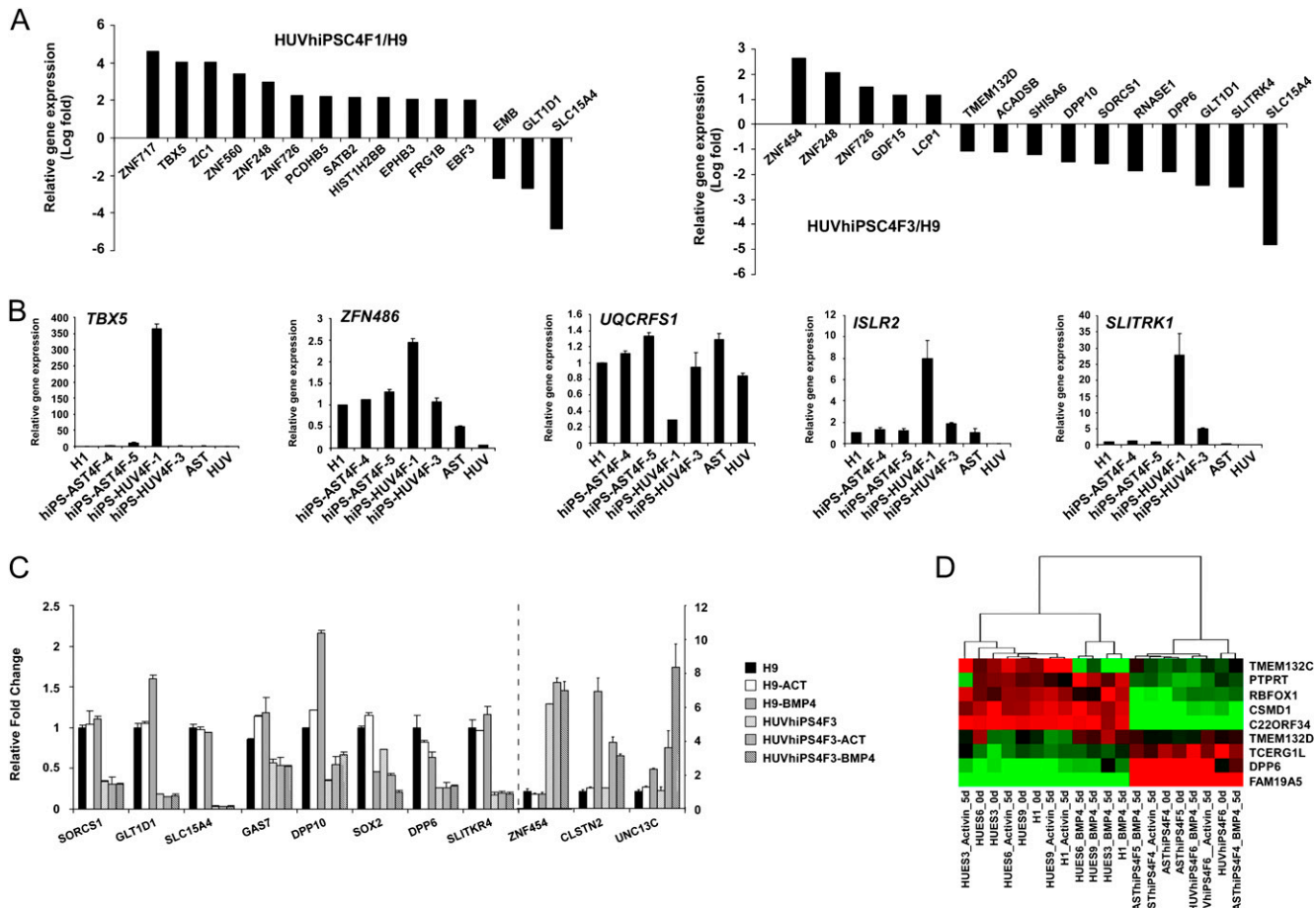


**Fig. S4.** Reprogramming-associated epigenetic/transcriptional signatures segregate hiPSCs and hESCs after differentiation. (A) Graph showing the relative log-fold expression change of genes adjacent to aberrantly methylated CpG sites in HUVhiPSC4F1 and HUVhiPSC4F3 compared with H9 cells. Data were obtained from microarray analysis and only the most differentially expressed genes are shown. (B) Real-time PCR analysis of genes adjacent to CpGs sites that showed hiPSC line-specific (HUVhiPSC4F1) epigenetic aberrations. Gene expression values were normalized to the levels observed in the H1 hESC line. Data are shown as relative averages  $\pm$  SD of two biological replicates analyzed in triplicate. (C) Genes with aberrantly methylated CpG sites and differential transcriptional abundance with at least a twofold cutoff were identified in the HUVhiPSC4F3 cell line after comparison with H9 cells. Graph shows the relative fold change in the expression of genes still aberrantly methylated after differentiation between the differentiated HUVhiPSC4F3 cell line and the differentiated hESC cell line. Note that differential expression was independent on whether Activin or BMP4-differentiated cells were analyzed. (D) Hierarchical clustering of hESC (H1, HUES3, HUES6, and HUES9) and hiPSC (ASThiPSC4F4, ASThiPSC4F5, and HUVhiPSC4F6) in their pluripotent and differentiated states based on the gene expression level of the nine common aberrantly methylated genes identified in the hiPSC lines used in this study. The clustering was generated by using the gene expression level analyzed by real-time PCR of the nine common aberrantly methylated genes identified in hiPSC lines used in this study.

Table S1. Summary table for the cell lines used in this study and methylation statistics

Sample	Laboratory of generation	Reprogramming experiment	Reprog. factors retroviral transduction or treatment	Passage no.	Reprog. efficiency, %	Raw base pairs sequenced methylome	No. of individual CpG sites
Keratinocytes	—	—	—	3	—	1,646,570,700	553,563
KhiPS4FA	JCBI/SALK	Experiment 1	Oct4, Sox2, Klf4 and cMyc	54	~0.1–1	1,689,864,600	496,310
K.MMTA (human foreskin keratinocytes)	—	—	—	5	—	1,268,486,320	152,644
KhiPS4F8	JCBI/CMRB	Experiment 1	Oct4, Sox2, Klf4 and cMyc	28	~0.1–1	1,234,677,920	168,359
Astrocytes (human astrocytes)	—	—	—	12	—	1,451,440,400	872,457
ASThiPS4F1	JCBI/SALK	Experiment 1	Oct4, Sox2, Klf4 and cMyc	12	~0.1–1	3,909,632,900	729,294
ASThiPS4F2	JCBI/SALK	Experiment 1	Oct4, Sox2, Klf4 and cMyc	12	~0.1–1	2,912,954,300	696,530
ASThiPS4F3	JCBI/SALK	Experiment 1	Oct4, Sox2, Klf4 and cMyc	24	~0.1–1	2,898,925,300	617,223
ASThiPS4F4	JCBI/SALK	Experiment 1	Oct4, Sox2, Klf4 and cMyc	10	~0.1–1	3,333,550,100	853,766
ASThiPS4F5	JCBI/SALK	Experiment 1	Oct4, Sox2, Klf4 and cMyc	10	~0.1–1	1,761,937,540	887,230
HUVEC (human umbilical vein endothelial cells)	—	—	—	2	—	4,004,776,700	683,024
HUVhiPS4F1	JCBI/SALK	Experiment 1	Oct4, Sox2, Klf4 and cMyc	20	~2.5–3	1,335,321,790	833,100
HUVhiPS4F3	JCBI/SALK	Experiment 2	Oct4, Sox2, Klf4 and cMyc	15	~2.5–3	1,550,482,890	944,367
HUVhiPS4F6	JCBI/SALK	Experiment 2	Oct4, Sox2, Klf4 and cMyc	23	~2.5–3	2,916,794,200	691,180
hNSC (human neural stem cells)	—	—	—	N.D.	—	1,443,904,880	180,815
NSChiPS2F	HRS;MPIMB	Experiment 1	Oct4 and Klf4	23	~0.006	1,500,813,280	160,868
IMR90 (human fibroblasts)	—	—	—	6	—	1,871,225,800	580,915
FhiPS4F2	JCBI/SALK	Experiment 1	Oct4, Sox2, Klf4 and cMyc	32	~0.01	3,326,510,300	742,667
FhiPS4F5	JCBI/SALK	Experiment 2	Oct4, Sox2, Klf4 and cMyc	29	~0.01	1,859,256,500	536,878
HFF-XF (human fibroblasts)	—	—	—	N.D.	—	1,096,105,680	143,049
FhiPS4F7	JCBI/CMRB	Experiment 1	Oct4, Sox2, Klf4 and cMyc	9	~0.01	1,391,285,360	174,060
PGP1F (human adult fibroblasts)	—	—	—	9	—	3,684,432,620	563,424
PGP1-hiPS	GC/HMS	Experiment 1	Oct4, Sox2, Klf4 and cMyc	16	~0.001	3,298,612,900	479,778
MSC (mesenchymal stem cells)	—	—	—	7	—	3,451,992,720	366,816
MSChiPS4	JCBI/CMRB	Experiment 1	Oct4, Sox2, Klf4 and cMyc	14	N.D.	3,722,264,000	785,501
MSChiPS8	JCBI/CMRB	Experiment 1	Oct4, Sox2, Klf4 and cMyc	14	N.D.	3,287,020,500	766,374
HUES2	—	—	—	41	—	4,109,799,200	742,407
HUES3	—	—	—	33	—	2,528,235,500	580,251
HUES6	—	—	—	26	—	2,182,207,100	646,752
HUES8	—	—	—	35	—	2,584,672,100	682,799
HUES9	—	—	—	36	—	3,055,997,100	655,730
hESC-H1	—	—	—	44	—	1,903,744,100	506,653
hESC-H9	—	—	—	42	—	2,258,101,100	588,686
ASThiPS4F5	—	—	ACTIVIN	16	—	2,294,425,700	640,530
ASThiPS4F4	—	—	ACTIVIN	36	—	2,889,037,800	669,426
HUVhiPS4F6	—	—	ACTIVIN	23	—	1,899,377,100	530,459
HUVhiPS4F1	—	—	ACTIVIN	20	—	3,866,644,100	800,144
HUVhiPS4F3	—	—	ACTIVIN	20	—	3,523,342,800	813,452
ASThiPS4F4	—	—	BMP4	36	—	2,884,287,100	692,467
ASThiPS4F5	—	—	BMP4	12	—	2,074,788,400	566,406
HUVhiPS4F6	—	—	BMP4	23	—	2,775,359,400	745,988
HUVhiPS4F1	—	—	BMP4	20	—	3,740,369,100	842,497
HUVhiPS4F3	—	—	BMP4	20	—	3,364,378,100	852,646
ASThiPS4F5	—	—	No treatment	16	—	2,576,713,500	670,394
ASThiPS4F4	—	—	No treatment	36	—	2,188,937,900	775,653
ASThiPS4F5	—	—	No treatment	12	—	2,936,136,900	749,230
HUVhiPS4F6	—	—	No treatment	23	—	2,891,450,800	657,282
HUVhiPS4F1	—	—	No treatment	19	—	3,556,673,300	854,660
HUVhiPS4F3	—	—	No treatment	19	—	3,309,173,000	836,711
HUES6	—	—	ACTIVIN	39	—	4,565,100,900	692,678
HUES9	—	—	ACTIVIN	39	—	4,505,094,000	779,397
HUES3	—	—	ACTIVIN	36	—	1,945,225,600	582,737
H1	—	—	ACTIVIN	54	—	2,799,394,800	645,398
H9	—	—	ACTIVIN	43	—	3,386,728,300	707,044
HUES6	—	—	BMP4	39	—	4,797,928,600	782,213
HUES9	—	—	BMP4	39	—	3,706,677,100	779,860

**Table S1. Cont.**

Sample	Laboratory of generation	Reprogramming experiment	Reprog. factors retroviral transduction or treatment	Passage no.	Reprog. efficiency, %	Raw base pairs sequenced	No. of individual methylome CpG sites
HUES3	—	—	BMP4	36	—	2,389,715,600	598,499
H1	—	—	BMP4	47	—	2,405,924,900	610,493
H9	—	—	BMP4	43	—	3,184,532,100	830,532
HUES6	—	—	No treatment	39	—	4,789,721,200	763,620
HUES9	—	—	No treatment	39	—	4,456,502,900	805,508
HUES3	—	—	No treatment	36	—	3,437,806,100	680,065
H1	—	—	No treatment	54	—	2,551,516,700	635,771
H1	—	—	No treatment	47	—	1,949,035,200	549,422
H9	—	—	No treatment	43	—	3,356,314,300	839,472

CMRB, Center of Regenerative Medicine in Barcelona; GC, George Church; HRS, Hans R. Schöler; JCBI, Juan Carlos Izpisua-Belmonte; MPIMB: Max Planck Institute for Molecular Biomedicine; N.D., not determined; SALK: SALK Institute for Biological Studies; HMS: Harvard Medical School.

**Table S2. CpG sites targeted in this study are more informative than those targeted in previous studies**

Sample	No. of DMSs	DMS, %	Unique DMS
Targeted sequencing of chosen sites			
ASThiPS4F1	45,467	27	82
ASThiPS4F2	44,379	26	103
ASThiPS4F3	46,112	27	262
ASThiPS4F4	43,457	25	58
ASThiPS4F5	41,900	24	110
FhiPS4F2	58,168	35	449
FhiPS4F5	59,266	35	661
FhiPS4F7	54190	32	1,428
HUVhiPS4F1	40,926	24	349
HUVhiPS4F3	40,768	24	366
HUVhiPS4F6	41,697	24	228
KhiPS4FA	49,432	29	1,337
KhiPS4F8	45,924	27	631
MSChiPS4F4	63,976	37	442
MSChiPS4F8	61,842	36	420
NSChiPS2F	38,688	23	2,865
PGP1-iPS	60,820	36	2,286
Targeted sequencing of CpG islands			
BjiPS11	1,354	17	67
BjiPS12	1,437	18	124
IMR90iPS	1,675	21	401
hFib2iPS	1,542	19	386

More differential methylation is observed in the current data set than in previous targeted sequencing experiments. The CpG sites analyzed in this study are therefore more informative than those analyzed in previous studies. Current data is presented in this work. Data obtained from previous studies (1).

1. Kim K, et al. (2011) Donor cell type can influence the epigenome and differentiation potential of human induced pluripotent stem cells. *Nat Biotechnol* 29:1117–1119.

**Table S3. List of primers used in this study**

Primer name	Sequence	Purpose
DPP6-F	TTTCCAGCACACAGCAGAAC	Real-time PCR
DPP6-F	GATGGACCGGTACAGATGCT	Real-time PCR
TMEM132C-F	GCAGAACATCCCCATTGACT	Real-time PCR
TMEM132C-R	GGCGTACATCCCTATCTCCA	Real-time PCR
TMEM132D-F	CTGTTGGCCATTGGTCT	Real-time PCR
TMEM132D-R	TTGCTTAACCCAAACCCAGTC	Real-time PCR
C22ORF34-F	GTGAAGGCCCCCTACACAAA	Real-time PCR
C22ORF34-R	CTAATTAGCGCAGCCTCACC	Real-time PCR
FAM19A5-F	TGTGTGACGAAGAATCAT	Real-time PCR
FAM19A5-R	GGAGACCGTGGTGGTCTTTA	Real-time PCR
PTPRT-F	GAGCCGACAAAGTTGCTTC	Real-time PCR
PTPRT-R	TGCTTGAGGGCACTTCCTT	Real-time PCR
PTPRN2-F	GGGTGAAAAGCAAACCTCAA	Real-time PCR
PTPRN2-R	GCAGTAGATGAGGCCAGAGG	Real-time PCR
RBFOX1-F	TGCTTTGCACCTTGACTG	Real-time PCR
RBFOX1-R	GGTTGTATCCCCCTCGGTAT	Real-time PCR
CSMD1-F	GCAAGTCTGGCTTCTCCATC	Real-time PCR
CSMD1-R	CACTGGAATGTGACGGTGTC	Real-time PCR
FRMD4B-F	ATAAAACCACCGTGGAGCTG	Real-time PCR
FRMD4B-R	AATCTCCCTGGCTTCCCTGT	Real-time PCR
TECRG1L-F	CCTGCTGTCTGGGAGAAC	Real-time PCR
TCERG1L-R	CATCGCTGTTGTCAGTTGCT	Real-time PCR
CNTN4-F	CGAGGCTTGGTTATGTTG	Real-time PCR
CNTN4-R	CACGCTCTCATTCTGAACA	Real-time PCR
C9ORF64-F	GCACCTGGTGGTTGAAAGTT	Real-time PCR
C9ORF64-R	GTCCITGAAGCAGCCATCTC	Real-time PCR
ISLR2-F	TGGACAAGTACGCTCACCA	Real-time PCR
ISLR2-R	CGCAGCACAGTGTATTTGTT	Real-time PCR
SLITRK1-F	GGACACAAGTCTGTTGGT	Real-time PCR
SLITRK1-R	GCTGAAAACATTCCAAGA	Real-time PCR
TBX5-F	TTGGATGAGGTGGAGAGAC	Real-time PCR
TBX5-R	GGAGCTGACAGAATGTCAA	Real-time PCR
ZFN486-F	CTGATCACCTGTCTGGACCA	Real-time PCR
ZFN486-R	GGTCTTGGGCAAATGAGAA	Real-time PCR
UQCRLS1-F	GCACCTTGATGTCTGTGG	Real-time PCR
UQCRLS1-R	AGCCTGTGTTGGACCTGAAG	Real-time PCR
AmpF6.4Sol	AATGATACGGCACCACCGAGATCTACACCACTCTCAGATGTTATCGAGGTCCGAC	Library-free BSPP primer
AmpR6.3Ind1	CAAGCAGAACAGGCATACGAGATCGTGTGCTAGGAACGATGAGCCTCAAAC	Library-free BSPP barcoded primer
AmpR6.3Ind2	CAAGCAGAACAGGCATACGAGATACATCGGCTAGGAACGATGAGCCTCAAAC	Library-free BSPP barcoded primer
AmpR6.3Ind3	CAAGCAGAACAGGCATACGAGATGCCAAGCTAGGAACGATGAGCCTCAAAC	Library-free BSPP barcoded primer
AmpR6.3Ind4	CAAGCAGAACAGGCATACGAGATTGGTCAGCTAGGAACGATGAGCCTCAAAC	Library-free BSPP barcoded primer
AmpR6.3Ind5	CAAGCAGAACAGGCATACGAGATCAGTGTGCTAGGAACGATGAGCCTCAAAC	Library-free BSPP barcoded primer
AmpR6.3Ind6	CAAGCAGAACAGGCATACGAGATATTGGCCTAGGAACGATGAGCCTCAAAC	Library-free BSPP barcoded primer
AmpR6.3Ind7	CAAGCAGAACAGGCATACGAGATGATCTGGCTAGGAACGATGAGCCTCAAAC	Library-free BSPP barcoded primer
AmpR6.3Ind8	CAAGCAGAACAGGCATACGAGATTCAGCAAGTGTAGGAACGATGAGCCTCAAAC	Library-free BSPP barcoded primer
AmpR6.3Ind9	CAAGCAGAACAGGCATACGAGATCTGATCGCTAGGAACGATGAGCCTCAAAC	Library-free BSPP barcoded primer
AmpR6.3Ind10	CAAGCAGAACAGGCATACGAGATAACGCTAGGAACGATGAGCCTCAAAC	Library-free BSPP barcoded primer
AmpR6.3Ind11	CAAGCAGAACAGGCATACGAGATGTCAGCGCTAGGAACGATGAGCCTCAAAC	Library-free BSPP barcoded primer
AmpR6.3Ind12	CAAGCAGAACAGGCATACGAGATTACAGAGCTAGGAACGATGAGCCTCAAAC	Library-free BSPP barcoded primer
AmpR6.3Ind13	CAAGCAGAACAGGCATACGAGATTCTGGCTAGGAACGATGAGCCTCAAAC	Library-free BSPP barcoded primer
AmpR6.3Ind14	CAAGCAGAACAGGCATACGAGATTGCTCTGCTAGGAACGATGAGCCTCAAAC	Library-free BSPP barcoded primer
AmpR6.3Ind15	CAAGCAGAACAGGCATACGAGATAGGAAGGCTAGGAACGATGAGCCTCAAAC	Library-free BSPP barcoded primer
AmpR6.3Ind16	CAAGCAGAACAGGCATACGAGATAACCCGCTAGGAACGATGAGCCTCAAAC	Library-free BSPP barcoded primer
AmpR6.3Ind17	CAAGCAGAACAGGCATACGAGATGATGAGGCTAGGAACGATGAGCCTCAAAC	Library-free BSPP barcoded primer
AmpR6.3Ind18	CAAGCAGAACAGGCATACGAGATTGAACGATGAGCCTCAAAC	Library-free BSPP barcoded primer
AmpR6.3Ind19	CAAGCAGAACAGGCATACGAGATTGCGTCGCTAGGAACGATGAGCCTCAAAC	Library-free BSPP barcoded primer
AmpR6.3Ind20	CAAGCAGAACAGGCATACGAGATGACAGGGCTAGGAACGATGAGCCTCAAAC	Library-free BSPP barcoded primer
AmpR6.3Ind21	CAAGCAGAACAGGCATACGAGATGGGTTGGCTAGGAACGATGAGCCTCAAAC	Library-free BSPP barcoded primer
AmpR6.3Ind22	CAAGCAGAACAGGCATACGAGATTCCGAGGCTAGGAACGATGAGCCTCAAAC	Library-free BSPP barcoded primer
AmpR6.3Ind23	CAAGCAGAACAGGCATACGAGATTTCGAGCTAGGAACGATGAGCCTCAAAC	Library-free BSPP barcoded primer
AmpR6.3Ind24	CAAGCAGAACAGGCATACGAGATGCAATGCTAGGAACGATGAGCCTCAAAC	Library-free BSPP barcoded primer
AmpR6.3Ind25	CAAGCAGAACAGGCATACGAGATGCAAGTAGCTAGGAACGATGAGCCTCAAAC	Library-free BSPP barcoded primer
AmpR6.3Ind26	CAAGCAGAACAGGCATACGAGATTACGAGCTAGGAACGATGAGCCTCAAAC	Library-free BSPP barcoded primer

**Table S3. Cont.**

Primer name	Sequence	Purpose
AmpR6.3Ind27	CAAGCAGAAGACGGCATAACGAGATCGCTAGCTAGGAACGATGAGCCTCCAAC	Library-free BSPP barcoded primer
AmpR6.3Ind28	CAAGCAGAAGACGGCATAACGAGATGCCCTGCTAGGAACGATGAGCCTCCAAC	Library-free BSPP barcoded primer
AmpR6.3Ind29	CAAGCAGAAGACGGCATAACGAGATCTTCGCTAGGAACGATGAGCCTCCAAC	Library-free BSPP barcoded primer
AmpR6.3Ind30	CAAGCAGAAGACGGCATAACGAGATCACTAACGCTAGGAACGATGAGCCTCCAAC	Library-free BSPP barcoded primer
AmpR6.3Ind31	CAAGCAGAAGACGGCATAACGAGATGTTGGCTAGGAACGATGAGCCTCCAAC	Library-free BSPP barcoded primer
AmpR6.3Ind32	CAAGCAGAAGACGGCATAACGAGATCCTTCGCTAGGAACGATGAGCCTCCAAC	Library-free BSPP barcoded primer
AmpR6.3Ind33	CAAGCAGAAGACGGCATAACGAGATGTTGGCTAGGAACGATGAGCCTCCAAC	Library-free BSPP barcoded primer
AmpR6.3Ind34	CAAGCAGAAGACGGCATAACGAGATTCAGTTGCTAGGAACGATGAGCCTCCAAC	Library-free BSPP barcoded primer
AmpR6.3Ind35	CAAGCAGAAGACGGCATAACGAGATCCCGATGCTAGGAACGATGAGCCTCCAAC	Library-free BSPP barcoded primer
AmpR6.3Ind36	CAAGCAGAAGACGGCATAACGAGATTGCTGGCTAGGAACGATGAGCCTCCAAC	Library-free BSPP barcoded primer
AmpR6.3Ind37	CAAGCAGAAGACGGCATAACGAGATTGAGCTAGGAACGATGAGCCTCCAAC	Library-free BSPP barcoded primer
AmpR6.3Ind38	CAAGCAGAAGACGGCATAACGAGATCGCTGAGCTAGGAACGATGAGCCTCCAAC	Library-free BSPP barcoded primer
AmpR6.3Ind39	CAAGCAGAAGACGGCATAACGAGATCTGGCTAGGAACGATGAGCCTCCAAC	Library-free BSPP barcoded primer
AmpR6.3Ind40	CAAGCAGAAGACGGCATAACGAGATCCGTACAGTAGGAACGATGAGCCTCCAAC	Library-free BSPP barcoded primer
AmpR6.3Ind41	CAAGCAGAAGACGGCATAACGAGATGTTCCGCTAGGAACGATGAGCCTCCAAC	Library-free BSPP barcoded primer
AmpR6.3Ind42	CAAGCAGAAGACGGCATAACGAGATCTTCGCTAGGAACGATGAGCCTCCAAC	Library-free BSPP barcoded primer
AmpR6.3Ind43	CAAGCAGAAGACGGCATAACGAGATGGCACTGCTAGGAACGATGAGCCTCCAAC	Library-free BSPP barcoded primer
AmpR6.3Ind44	CAAGCAGAAGACGGCATAACGAGATGGATGCGCTAGGAACGATGAGCCTCCAAC	Library-free BSPP barcoded primer
AmpR6.3Ind45	CAAGCAGAAGACGGCATAACGAGATCGTAGTGTAGGAACGATGAGCCTCCAAC	Library-free BSPP barcoded primer
AmpR6.3Ind46	CAAGCAGAAGACGGCATAACGAGATGGAAATGGCTAGGAACGATGAGCCTCCAAC	Library-free BSPP barcoded primer
AmpR6.3Ind47	CAAGCAGAAGACGGCATAACGAGATGGAGAGGCTAGGAACGATGAGCCTCCAAC	Library-free BSPP barcoded primer
AmpR6.3Ind48	CAAGCAGAAGACGGCATAACGAGATTACGTGCTAGGAACGATGAGCCTCCAAC	Library-free BSPP barcoded primer
AmpR6.3Ind49	CAAGCAGAAGACGGCATAACGAGATACAGGCTAGGAACGATGAGCCTCCAAC	Library-free BSPP barcoded primer
AmpR6.3Ind50	CAAGCAGAAGACGGCATAACGAGATAAGGTGCTAGGAACGATGAGCCTCCAAC	Library-free BSPP barcoded primer
AmpR6.3Ind51	CAAGCAGAAGACGGCATAACGAGATCGATAGCTAGGAACGATGAGCCTCCAAC	Library-free BSPP barcoded primer
AmpR6.3Ind52	CAAGCAGAAGACGGCATAACGAGATCGTAGTGTAGGAACGATGAGCCTCCAAC	Library-free BSPP barcoded primer
AmpR6.3Ind53	CAAGCAGAAGACGGCATAACGAGATGTAAGACTAGGAACGATGAGCCTCCAAC	Library-free BSPP barcoded primer
AmpR6.3Ind54	CAAGCAGAAGACGGCATAACGAGATGGACGTGCTAGGAACGATGAGCCTCCAAC	Library-free BSPP barcoded primer
AmpR6.3Ind55	CAAGCAGAAGACGGCATAACGAGATAGTCGAGCTAGGAACGATGAGCCTCCAAC	Library-free BSPP barcoded primer
AmpR6.3Ind56	CAAGCAGAAGACGGCATAACGAGATGTCGAGCTAGGAACGATGAGCCTCCAAC	Library-free BSPP barcoded primer
AmpR6.3Ind57	CAAGCAGAAGACGGCATAACGAGATGAAGGAGCTAGGAACGATGAGCCTCCAAC	Library-free BSPP barcoded primer
AmpR6.3Ind58	CAAGCAGAAGACGGCATAACGAGATATGCTGGCTAGGAACGATGAGCCTCCAAC	Library-free BSPP barcoded primer
AmpR6.3Ind59	CAAGCAGAAGACGGCATAACGAGATTCTATCGTAGGAACGATGAGCCTCCAAC	Library-free BSPP barcoded primer
AmpR6.3Ind60	CAAGCAGAAGACGGCATAACGAGATATCTGTGCTAGGAACGATGAGCCTCCAAC	Library-free BSPP barcoded primer
AmpR6.3Ind65	CAAGCAGAAGACGGCATAACGAGATAAGGAAGCTAGGAACGATGAGCCTCCAAC	Library-free BSPP barcoded primer
AmpR6.3Ind66	CAAGCAGAAGACGGCATAACGAGATCCTCCACGCTAGGAACGATGAGCCTCCAAC	Library-free BSPP barcoded primer
AmpR6.3Ind69	CAAGCAGAAGACGGCATAACGAGATCCATATGCTAGGAACGATGAGCCTCCAAC	Library-free BSPP barcoded primer
AmpR6.3Ind70	CAAGCAGAAGACGGCATAACGAGATGAAGTCGCTAGGAACGATGAGCCTCCAAC	Library-free BSPP barcoded primer
AmpR6.3Ind71	CAAGCAGAAGACGGCATAACGAGATAAAAGAGCTAGGAACGATGAGCCTCCAAC	Library-free BSPP barcoded primer
AmpF6.3NH2	/5AmMC6/CAGATGTTATCGAGGTCGAC (5' Amino modifier C6)	Padlock probe amplification
AmpR6.3NH2	/5AmMC6/GGAACGATGAGCCTCCAC (5' Amino modifier C6)	Padlock probe amplification
PE_t_N2	ACACTCTTCCTACACGACGCTCTCCGATCTN* N 3'-Phosphorothioate bond	Padlock probe library construction
PE_b_A	/5Phos/AGATCGGAAGAGCGGTTACAGCAGGAATGCCGAG 5'-Phosphorylation	Padlock probe library construction

BSPP, bisulfite padlock probe.

## Other Supporting Information Files

- [Dataset S1 \(XLS\)](#)
- [Dataset S2 \(XLS\)](#)
- [Dataset S3 \(XLS\)](#)